

# Jet Constituents for Deep Neural Network Based Top Quark Tagging

J. Pearkes, W. Fedorko, A. Lister, C. Gay<sup>1</sup>

<sup>1</sup>*Department of Physics and Astronomy,  
The University of British Columbia, BC, Canada*

(Dated: July 17, 2022)

## Abstract

Recent literature on deep neural networks for tagging of highly energetic jets resulting from top quark decays has focused on image based techniques or multivariate approaches using high level jet substructure variables. Here a sequential approach to this task is taken by using an ordered sequence of jet constituents as training inputs. Unlike previous approaches, this strategy does not result in a loss of information during pixelisation or the calculation of high level features. New preprocessing methods that do not alter key physical quantities such as the jet mass are developed. The jet classification method achieves background rejection of 45 for 50% efficiency operating point for reconstruction level jets with transverse momentum range of 600 to 2500 GeV and is insensitive to multiple proton-proton interactions at the levels expected throughout LHC Run 2.

## I. INTRODUCTION

The use of boosted top tagging algorithms in both searches and measurements is becoming more prevalent as the LHC datasets are increasing, thus extending the mass reach for searches involving new particles with top quark in their topology. Some recent examples from ATLAS and CMS include the search for new resonances decaying to top pairs in the all-hadronic and semi-leptonic top decay channels [1–3], searches for vector-like quarks in decays of  $T \rightarrow Ht$  [4],  $T \rightarrow Zt$  [5] or  $B \rightarrow Wt$ , searches for excited  $b$  quarks [6], and measurements of the differential cross section of top quark pair production in the all-hadronic channel [7, 8]. These analyses identify boosted top quarks via selection criteria applied to large radius jets (typically with  $R^1$  parameter of 0.8 or 1.0). In addition to the requirements that these jets have high momentum (typically above a couple of hundred GeV), the majority of analyses impose an additional requirement based on the invariant mass of the jet and on explicit requirements on jet substructure variables, such as  $\tau_{32}$ ,  $D_{32}$  and  $D_{12}$ . This is done to reject the non-top Quantum Chromodynamics (QCD) background, in which the jets originate from a lighter quark or gluon. Similar techniques have been applied to the identification of boosted vector bosons, which have also been used in a number of recent results such as Ref. [9].

The relative performance of a number of sub-structure based techniques have been studied in both ATLAS [10] and CMS [11]. Typical performances for the best top taggers have background rejection ratios of order 15 or 5 for signal efficiencies of 50% or 80%, respectively, for jets around 1 TeV in transverse momentum  $p_T$ .

In the past couple of years there has been a number of studies using Deep Learning techniques to improve the performance of boosted top,  $W$ ,  $Z$  or Higgs tagging. One of the first papers looked at the use of jet images and techniques derived from computer vision (such as facial recognition algorithms) to gain further insight on the structure of boosted hadronic  $W$  boson decays [12]; this study was carried out using Monte Carlo particle-level information and obtained a 20% improvement in the background rejection over a more traditional N-subjettiness ratio ( $\tau_2/\tau_1$ ). This idea was further developed and applied to the hadronic decay of top quarks where a 4% mistag rate (background rejection of 25) was achieved for 60% signal efficiency in jets with transverse momentum around 1000 GeV [13]. A later paper further develops this jet-image processing on  $W$  boson decays by including modern deep neural networks (DNN) [14]; for jet transverse momenta around 250 GeV, a rejection factor of 7 is obtained for 50% signal efficiency. Using a mixture of locally-connected and fully-connected nodes in a deep neural network architecture, again applied to  $W$  boson identification, another study was able to get a rejection rate of about 100 for a 50% signal efficiency [15]. This was obtained for jets with transverse momenta between 300 and 400 GeV and showed similar performance to a more traditional boosted decision tree (BDT) trained on six high-level variables. There has also been some work to extend these ideas to jet flavour, in particular  $b$ -jet identification [16]. While many of these studies

---

<sup>1</sup> In this article a cylindrical coordinate system is adopted with the  $z$  axis along the beamline. Polar angle is  $\theta$ , azimuthal angle is  $\phi$ . Transverse momentum  $p_T$  is the component of particle momentum in the  $x - y$  plane. Pseudorapidity  $\eta$  is defined as  $\eta = -\ln\left(\tan\left(\frac{\theta}{2}\right)\right)$ . Distance  $R$  in  $\eta - \phi$  space is defined as  $R = \sqrt{\Delta\eta^2 + \Delta\phi^2}$

did include the study of the impact of large numbers of additional interactions (pileup), they were performed using stable particles, i.e. without including any impact of a detector resolution or efficiency. Ref. [15] did bin their jet images into pixels to form 32x32 pixel images, thus approximating the resolution of the calorimeter. In order to better understand how applicable such techniques are to real LHC collision data, the performance of a deep learning algorithm was studied on  $W$  boson tagging under variations of the parton shower model [17]. The performance was found to vary by up to 50% using a DELPHES [18] detector simulation.

The use of Generative Adversarial Network (GAN) on jet images is explored in Ref.[19]. Another study on the identification of hadronic decays of boosted top quarks using convolutional neural networks includes the expected impact of a finite detector resolution using DELPHES assuming similar calorimeter granularity to that of the CMS detector [20]. A relatively low jet transverse momentum range from 350 to 400 GeV is explored, though a large jet parameter is chosen,  $R=1.5$ , presumably to ensure the top decay is fully contained. The performance of their best tagger, DeepTop, gives a rejection factor of  $\sim 40$  for a signal efficiency of 50%; it slightly out-performs their BDT based tagger, trained on high level substructure variables.

A recent paper [21] has taken an alternative look at the problem by using recursive neural networks built upon an analogy between QCD and natural language. Variable length sets of four-momenta are used as input to the training. The performance of this method on the identification of boosted  $W$  bosons, using calorimeter tower emulation, gives a background rejection factor of  $\sim 25$  for a 50% signal efficiency. The ideal performance using particles as input to the training is found to be  $\sim 70$  for the same efficiency.

The study of boosted event shapes for the identification of top, Higgs and vector bosons was studied in [22]. In particular a method is described to account for the momentum spread within a sample by boosting into the centre-of-mass frame of the original particle.

While much of the literature has so far focused on describing methods, most have used the performance of  $W$  boson identification as a benchmark, while only Refs. [13, 20, 22] have explored the performance of the algorithms top tagging.

Here a method based on a DNN is presented for discriminating top-quark originated jets, henceforth referred to as “signal”, from jets originating from all other quark flavours and gluons, henceforth referred to as “background”. The focus of this article are jets with  $p_T$  above 600 GeV up to 2500 GeV. In this regime, the  $R=1.0$  jets considered are expected to fully contain top quark decays. In Refs. [13, 20] deep convolutional neural network-based top tagging methods were developed drawing on the success of these techniques in image recognition. However as illustrated in Fig. 1, where energy deposits in signal and background jets are shown, the detector activation within a jet is sparse, with most of the detector area within the jet not being activated. No discernible features such as edges, corners or arcs are present. Convolutional networks therefore may not be the optimal architecture for top tagging. In this article, the performance of fully connected deep neural networks utilising four-vectors of jet constituents is examined. The data preprocessing techniques applied are described in section III. The performance of the network, the effects of preprocessing as well as the dependence of the performance on pileup is studied in section IV. The network was

implemented using the KERAS suite [23] with the THEANO [24] backend.

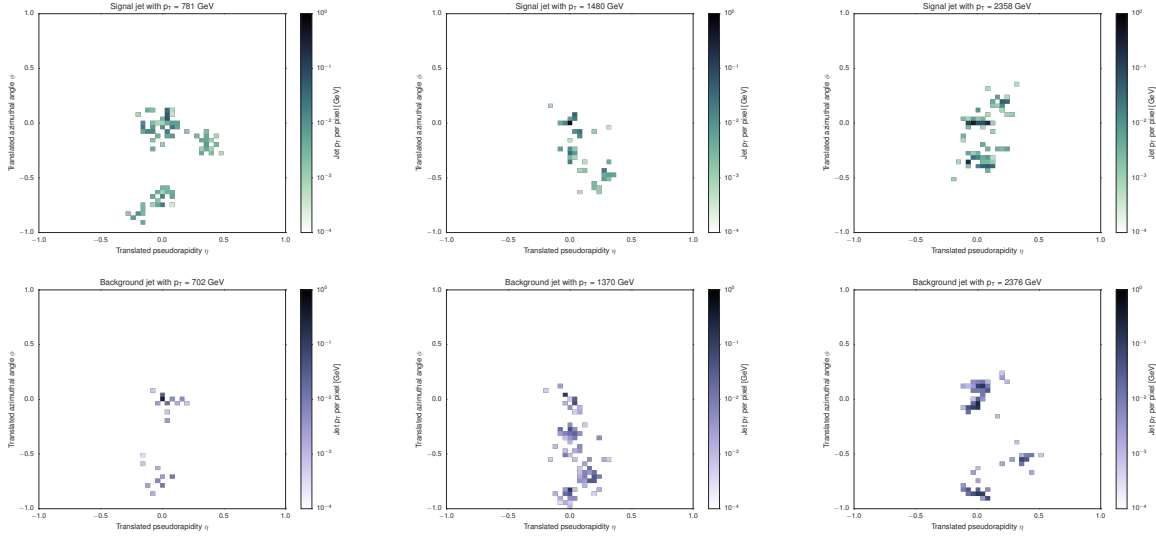


FIG. 1. Histograms of the fraction of jet  $p_T$  carried by constituents in  $\eta - \phi$  space for examples of signal and background jets. Jets were preprocessed as described in section III.

## II. DATASET

### A. Signal and background modelling

The modelling of jets resulting from hadronic top quark decays as well as gluon and light-flavour jets relies on Monte Carlo (MC) simulation. All processes are generated at leading order (LO) using the A14 tune [25] of the PYTHIA v8.219 [26] event generator with the NNPDF23\_LO\_AS\_0130\_QED PDF set, implemented in the LHAPDF package [27]. The hard scattering process, hadronisation and showering are simulated in a single step.

Samples of Sequential Standard Model  $Z'$  boson [28] production at the LHC with pole masses ranging in 32 steps from 1400 to 6360 GeV are generated. A centre-of-mass energy cut is applied at 90% of the  $Z'$  boson pole mass as well as a cut on the top quark  $p_T$  proportional to the  $Z'$  pole mass. These cuts are applied to ensure that the top-jet pseudorapidity distribution approximately matches that of the background jets. Only the  $Z'$  decay to  $t\bar{t}$  final state is permitted with each top quark decaying hadronically. Similarly, hard QCD “dijet”  $2 \rightarrow 2$  processes, incorporating gluon-gluon, quark-quark and quark-gluon scattering are generated in 32 bins of the outgoing parton transverse momentum ranging from 470 to 2790 GeV. Outgoing partons can be gluons as well as all quark flavours except for top. Only light flavour quarks are treated as massless in the matrix element. A large sample of inelastic, non-diffractive soft QCD events, commonly referred to as minimum bias is also generated.

The detector response is simulated using the DELPHES v3.4.0 suite [18] using the default emulation of the CMS detector. Minimum bias events are overlaid on the hard scattering

process to mimic “pileup”: multiple  $pp$  collisions occurring within single LHC bunch crossing. Three scenarios are simulated; in the first, no additional  $pp$  interactions are added. In the other two, a random number of additional  $pp$  collisions is overlaid; in one case the number is drawn from a Poisson distribution with mean of 23, approximately mimicking the pileup conditions of the LHC during the 2016 data-taking; the other case uses a Poisson distribution with a mean of 50, anticipating the pileup conditions at the end of the LHC Run 2. The case where an average of 23 pileup interactions are overlaid is referred to as the LHC 2016 pileup scenario below.

## B. Jet Selection

Large radius jets are formed from DELPHES energy-flow objects that emulate CMS particle-flow algorithm [29, 30]. The anti- $k_T$  algorithm [31] implemented by the FASTJET package [32] with radius parameter  $R=1.0$  is employed. A trimming procedure [33] is applied, where jet constituents are re-clustered into “subjets” using the  $k_T$  algorithm [34] with radius parameter  $R=0.2$  and constituents that belong to subjets carrying less than 5% of the jet transverse momentum are removed. Jet four-vectors are calculated using the remaining constituents. No further calibration or pileup subtraction steps are applied. For the simulation run with no pileup added, the jet finding and trimming is also performed on all stable particles output by the generator to evaluate the performance without detector effects.

Signal jets were truth matched such that the  $\Delta R$  between a hadronically decaying top quark and the large radius jet was less than 0.75. In addition, jets were selected to have  $\eta \leq 2.0$  and a jet  $p_T$  between 600 and 2500 GeV. After this pre-selection, the generated jets were subsampled in  $p_T$  and  $\eta$  to achieve a flat distribution in  $p_T$ , and a signal matched distribution in  $\eta$ . This step was taken to prevent the deep neural network from learning the underlying  $p_T$  and  $\eta$  distributions of the generated signal and background jets. This selection resulted in approximately 7.5 million jets (3.75 million signal jets and 3.75 million background jets). An additional independent set was also simulated and set aside for testing. After the selection described above this test set comprises 11 million jets evenly split between signal and background.

## C. Training, Validation and Test Samples

The 7 million jet sample was divided into training, validation and test sets in an 80%, 10%, 10% split. Decisions about which network architecture and preprocessing techniques were to be used were made by evaluating the best performance on the validation set. The test subset was used for the initial performance analysis. Evaluation of network performance at operating points corresponding to high background rejection justified the creation of the additional test set of 11 million jets. The sample is divided in 6 batches of 1.9 million jets each. In the network performance results quoted in section IV the first four batches (comprising 7.5 million jets) of this large test sample were used. To ascertain the impact of

the size of the test set on the quoted results, the performance metrics of the best performing network were evaluated on 15, 4-batch subsamples of the test set. This evaluation was performed only for the best performing network in the LHC 2016 pileup scenario due to computational constraints.

### III. NETWORK ARCHITECTURE

The input layer of the network consists of a vector of jet constituent  $p_T$ ,  $\eta$  and  $\phi$  coordinates. The network depth and number of nodes per layer were tuned manually, exploring a space between 4-6 layers and 40-1000 nodes per layer. ReLU activation [35] was used for the hidden layers while a sigmoid is used for the output node. The network was trained with the ADAM optimizer [36] for a minimum of 40 epochs. Early stopping with a patience parameter of 5 epochs on the validation set loss was used. The model used for evaluating the performance on the test set is the model with the best performance (lowest binary cross-entropy loss) on the validation set. This method prevents overtraining by freezing the model once performance on the validation set begins to decrease. The final chosen network architecture consisted of 4 hidden layers, with 300,102,12 and 6 nodes per layer. Figure 2 shows a schematic of the overall network architecture used in this study.

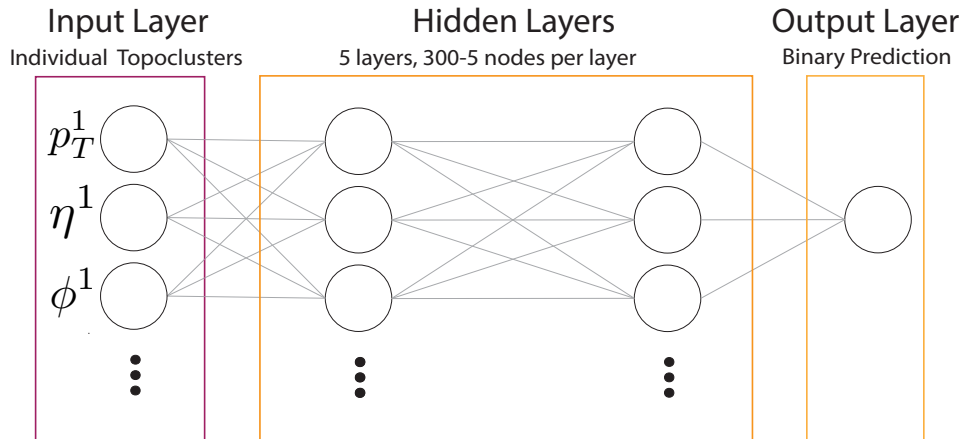


FIG. 2. Schematic of overall network architecture used.

#### A. Preprocessing

The key idea behind preprocessing the jets is that, by incorporating domain specific knowledge about the jet physics, the dimensionality of the problem can be reduced. The preprocessing steps were inspired by previous papers [14, 15, 17, 20] and determined through a series of studies. Jets are scaled, translated, rotated and flipped. First, the  $p_T$  of all jet constituents is scaled by 1700 to ensure that the majority of jet constituents have a  $p_T$

approximately between zero and one. This ensures that the value of the input nodes corresponding to the  $p_T$  of the jet constituents are roughly within the same order of magnitude as the input nodes corresponding to the  $\eta$  and  $\phi$  of the constituents. Next, jets are translated in  $\eta$  and  $\phi$  according to equations 1 and 2 so that their primary - highest  $p_T$  - subjet is centred about  $(0, 0)$ , that is the  $y$  and  $z$  components of the primary subjet are 0. In these and subsequent equations, subjet subscript 0 indicates the primary subjet, subscript 1 indicates the subjet with second highest  $p_T$  etc.

$$\eta'_{\text{constituent } n} = \eta_{\text{constituent } n} - \eta_{\text{subjet } 0} \quad (1)$$

$$\phi'_{\text{constituent } n} = \phi_{\text{constituent } n} - \phi_{\text{subjet } 0} \quad (2)$$

Unlike in previous studies [14, 15, 17, 20], the rotations are not performed directly in the  $\eta$ - $\phi$  plane as it results in a loss of jet mass information, as shown in Refs. [14, 20]. Instead, a rotation angle  $\vartheta$  about the x-axis is computed as shown in equation 3. The  $y$  and  $z$  components of all constituents are then transformed as shown in equations 4 and 5. This transformation results in the second highest  $p_T$  subjet being directly below the dominant subjet. This is a Lorentz transformation and therefore all the invariants such as the jet mass are preserved.

$$\vartheta = \tan^{-1}\left(\frac{p_{y, \text{subjet } 1}}{p_{z, \text{subjet } 1}}\right) + \frac{\pi}{2} \quad (3)$$

$$p'_{y, \text{constituent } n} = p_{y, \text{constituent } n} \cos \vartheta - p_{z, \text{constituent } n} \sin \vartheta \quad (4)$$

$$p'_{z, \text{constituent } n} = p_{y, \text{constituent } n} \sin \vartheta - p_{z, \text{constituent } n} \cos \vartheta \quad (5)$$

Finally, the jets are flipped in  $\eta$  if the average jet  $p_T$  lies on the left side on the  $\eta - \phi$  plane. The resulting jet constituents in each jet are ordered either by jet constituent  $p_T$  ( $p_T$ -ordering), or by subjet  $p_T$  and then jet constituent  $p_T$  (subjet ordering) and then presented to the neural network. The latter ordering is the primary choice selected in this article. As the sequences of  $(p_T, \eta, \phi)$  vary in length for each jet, the sequence was truncated at 120 jet constituents. This encompasses the majority of the jet constituents in each jet. Sequences were zero-padded when fewer than the maximum number of constituents are available.

Figure 3 shows the effect of the rotation and flip steps on  $\sim 400,000$  jets with  $p_T$  in the range between 600 and 700 GeV. These images represent the average jet image in this mass range. A noticeable difference between signal and background is the more densely populated 'halo' around the signal jets; this corresponds to the three-prong decay of the top quark.

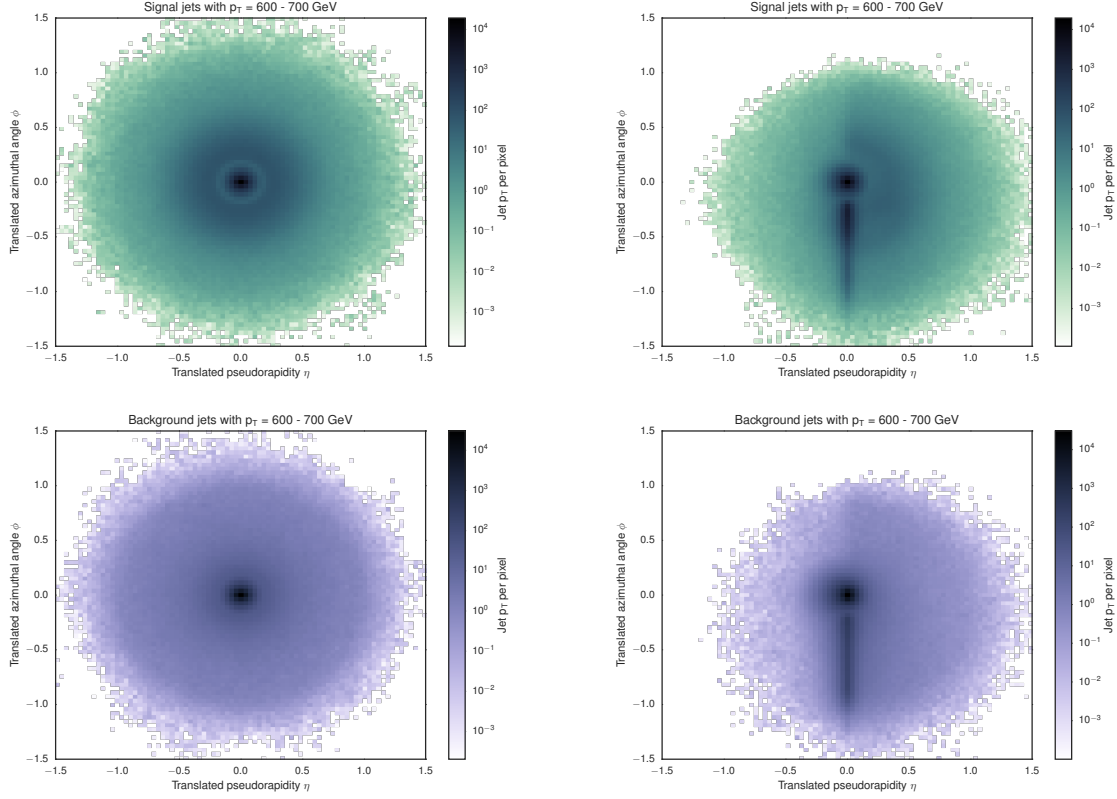


FIG. 3. Compound jet images before (left column) and after (right column) preprocessing for all signal (top row) and all background (bottom row) jets.

#### IV. PERFORMANCE ANALYSIS

Figure 4 shows Receiver Operating Characteristic (ROC) curves, for a deep neural network trained on reconstructed jets in the LHC 2016 pileup scenario as well as on truth jets without pileup. The ROC curve displays the dependency of the background rejection on the signal efficiency. Background rejection is defined as the inverse of the efficiency for accepting a background jet as signal, for a given operating point. Figure 4 also shows the performance on truth jets. The deep neural network trained and tested on truth jets outperforms the one trained and tested on reconstructed jets, but seems to have a milder degradation than what has been reported [21]. This difference in performance emphasizes the need for realistic detector simulation while designing methods for large  $R$ -jet tagging.

A commonly quoted measure of binary classifier performance is the Area Under the Curve (AUC). For a realistic physics analysis, a classifier operating point or a set of points would be picked depending on the expected signal yield as well as level of background contamination. To this end table I shows the AUC as well as the background rejection obtained for 20%, 50%, and 80% signal efficiency operating points. The resampling study, described in section II, found a standard deviation of  $10^{-4}$  for the AUC, 4 for the background rejection at 20% signal efficiency, 0.1 for the background rejection at 50% signal efficiency and 0.01 for the background rejection at 80% signal efficiency. In table I and subsequent tables the AUC is



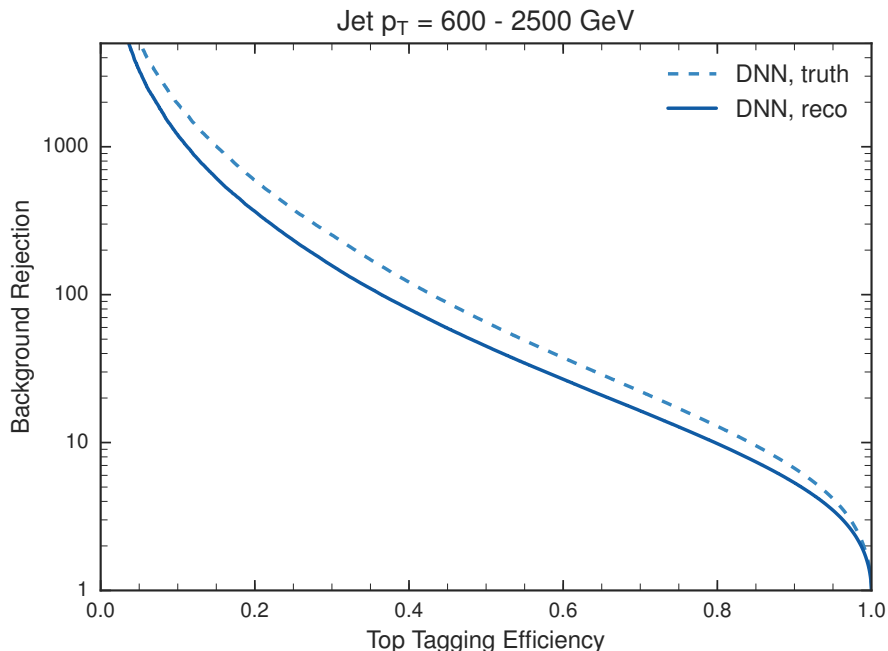


FIG. 4. The background rejection as a function of signal efficiency for the deep neural network. The performance on truth level (dashed line) as well as reconstruction level jets (labelled “reco”, solid line) is shown. For the reconstruction level jet sample, the LHC 2016 pileup scenario was used, for the truth jets, no pileup was added.

quoted to 3 significant figures, rejection at 20% signal efficiency is rounded to the nearest multiple of 5, the rejection at 50% signal efficiency is quoted to the nearest integer and the rejection at 80% signal efficiency is rounded to 0.1.

Jet sample	AUC	Rejection at signal efficiency of		
		20%	50%	80%
Reconstructed	0.934	365	45	9.8
Truth	0.946	595	65	12.9

TABLE I. Performance metrics for the DNN trained on reconstruction level and truth jets. For the reconstruction level jet sample, the LHC 2016 pileup scenario was used.

Of interest to physics analyses is the variation of the performance over a range of transverse momenta. In Figures 5 and 6 we show the performance at 80%, 50%, and 20% overall signal efficiency over the 600-2500 GeV range for reconstruction and truth level jets, respectively. The deep neural network displays a remarkably flat performance in signal efficiency. The performance in terms of background rejection is also relatively flat, though the rejection slightly increases between 600 GeV and approximately 1 TeV and then begins to decrease. Two effects may explain this; first a small fraction of top decay products may not be fully captured by the jet until very high momenta, and second, either the detector spatial resolu-

tion or the fixed  $R$  parameter of re-clustering may be causing jets at very high  $p_T$  to have altered structure with respect to jets at moderate momenta.

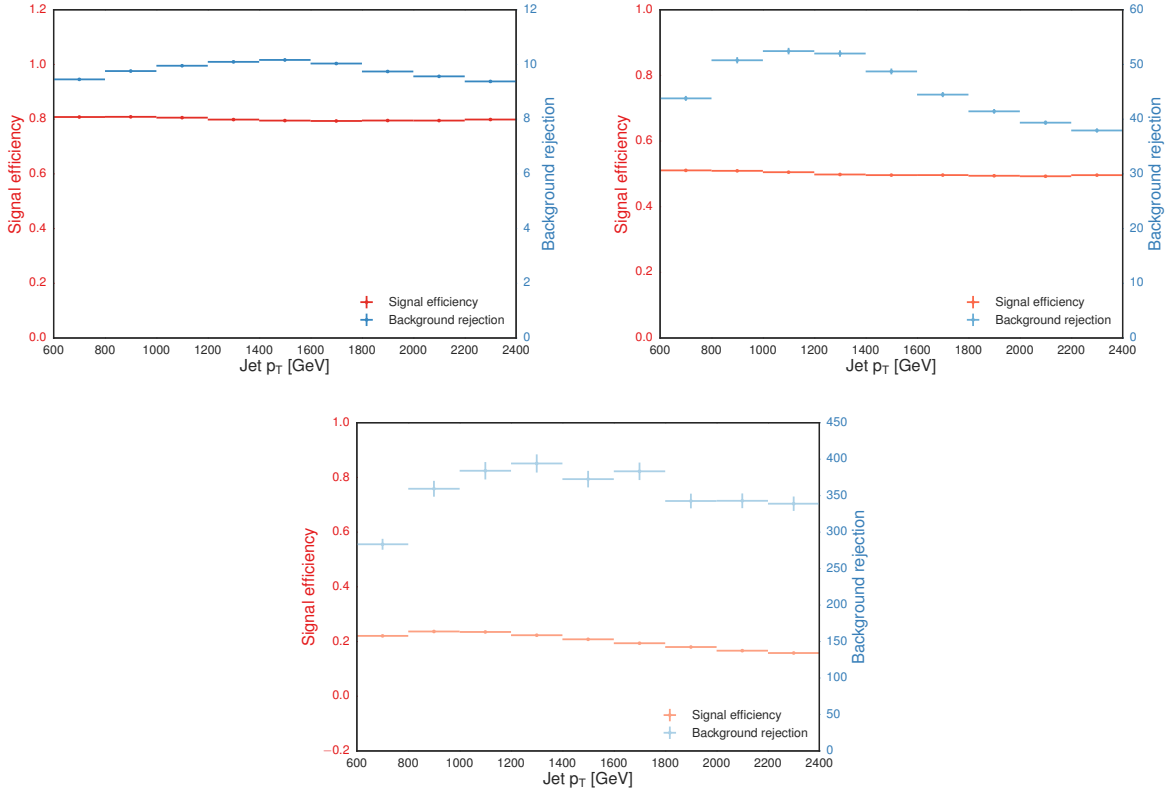


FIG. 5. Dependency of the top tagging efficiency (red) and background rejection (blue) on jet  $p_T$  for different overall signal efficiencies for reconstructed jets, assuming the LHC 2016 pileup scenario. Overall signal efficiency points of 80% (top left), 50% (top right) and 20% (bottom) are shown.

### A. Preprocessing Studies

The effect of multiple different preprocessing steps were studied to optimize the tagger performance. Figure 7 illustrates the performance gain from each sequential preprocessing step: trimming, scaling, translation, rotation and flipping. Each step has a positive impact on overall performance, with the final flipping step improving the performance only marginally. Table II summarizes the performance increase following each preprocessing stage.

The effect of trimming and jet constituent ordering was also investigated. Figure 8 shows the impact on the ROC curve of including or not the jet trimming, with all subsequent preprocessing stages applied in both cases. Trimmed jets typically perform better at the high background rejection operating point often desired in an analysis setting. Networks trained on jets without trimming perform marginally better at the signal efficiency operating

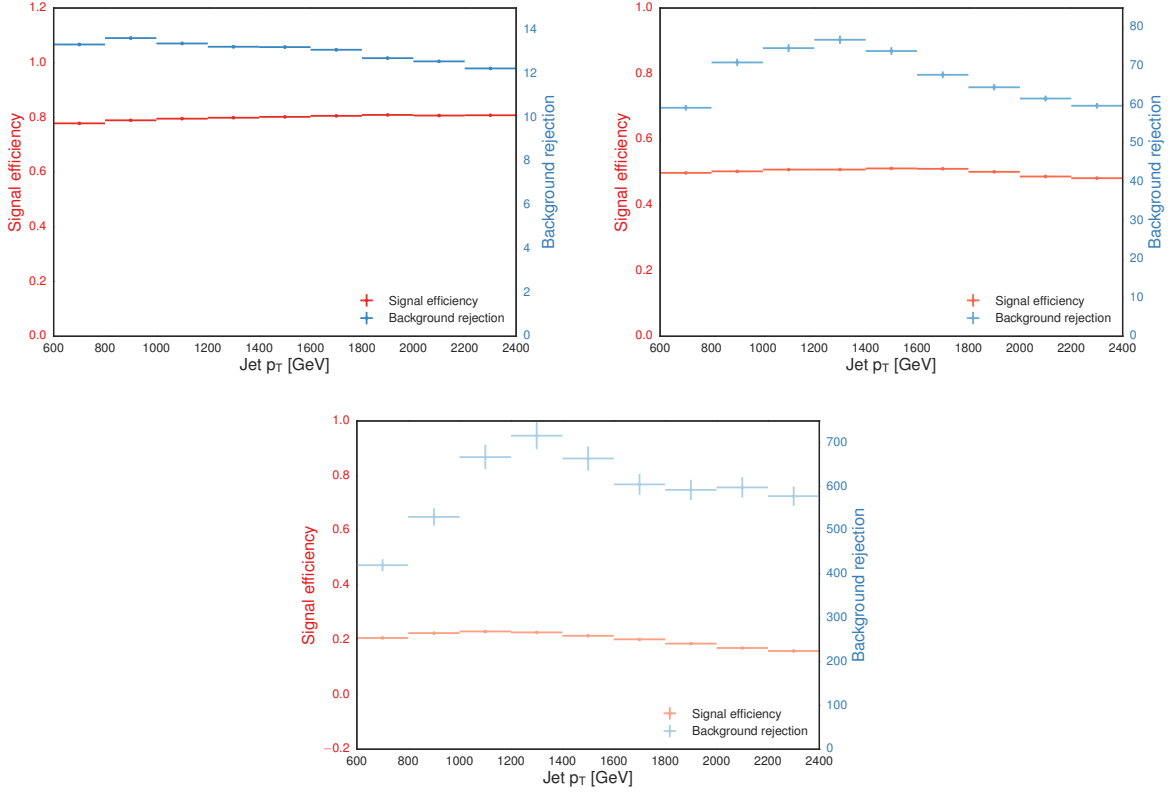


FIG. 6. Dependency of the top tagging efficiency (red) and background rejection (blue) on jet  $p_T$  for different overall signal efficiencies for truth particle jets, assuming no pileup. Overall signal efficiency points of 80% (top left), 50% (top right) and 20% (bottom) are shown.

Preprocessing stage	AUC	Rejection at signal efficiency of		
		20%	50%	80%
Trimming only	0.827	45	9	3.3
After scaling	0.904	130	22	6.3
After translation	0.920	175	30	7.9
After rotation	0.933	325	43	9.6
After flip	0.934	365	45	9.8

TABLE II. Performance metrics for the DNN trained on reconstruction level and truth jets after successive levels of preprocessing. A mean pileup of 23 was used.

points of approximately 65% and higher. The ordering has a very small effect on the overall performance, but subjet ordering was found to have the best performance. Details of the model performance for jet datasets with different trimming and constituent ordering are shown in table III.

The effect of three different types of boosting was also studied. This was inspired by [17] and [22] that use the ideas of scaling and boosting the jets, respectively, to reduce the

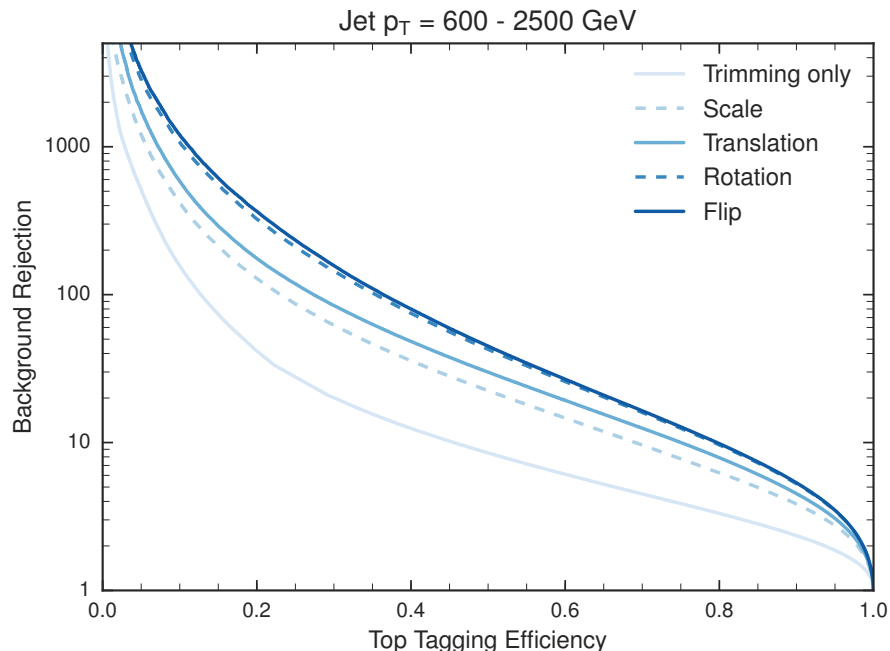


FIG. 7. ROC curve for DNN trained on reconstruction level jets after each successive preprocessing step, assuming a mean pileup of 23.

Trimming	Constituent ordering	AUC	Rejection at signal efficiency of		
			20%	50%	80%
Yes	subjet ordering	0.934	365	45	9.8
Yes	$p_T$ ordering	0.931	350	42	9.3
No	subjet ordering	0.937	265	42	10.2
No	$p_T$ ordering	0.934	260	40	9.6

TABLE III. Performance metrics for the DNN trained on reconstruction level jets with and without trimming and using subjet and  $p_T$  ordering. Successive preprocessing stages (scaling, translation, rotation and flipping) are applied for all cases. The LHC 2016 pileup scenario was used.

variability of jet substructure variables as a function of jet  $p_T$  and the “scale” of a jet image. In this study three approaches were tried: boosting the jet to its rest frame following [22], boosting the jet such that its  $p_T$  is identically 1000 GeV and boosting the jet so that the  $p_T$  of its primary subjet is always equal to the median  $p_T$  of the primary subjets of the top jets. None of the approaches yielded significant improvements in performance.

## B. Pileup studies

Pileup mitigation is of significant concern for the experiments at the LHC. Here the robustness of DNNs under different pileup conditions is studied. The model is trained and

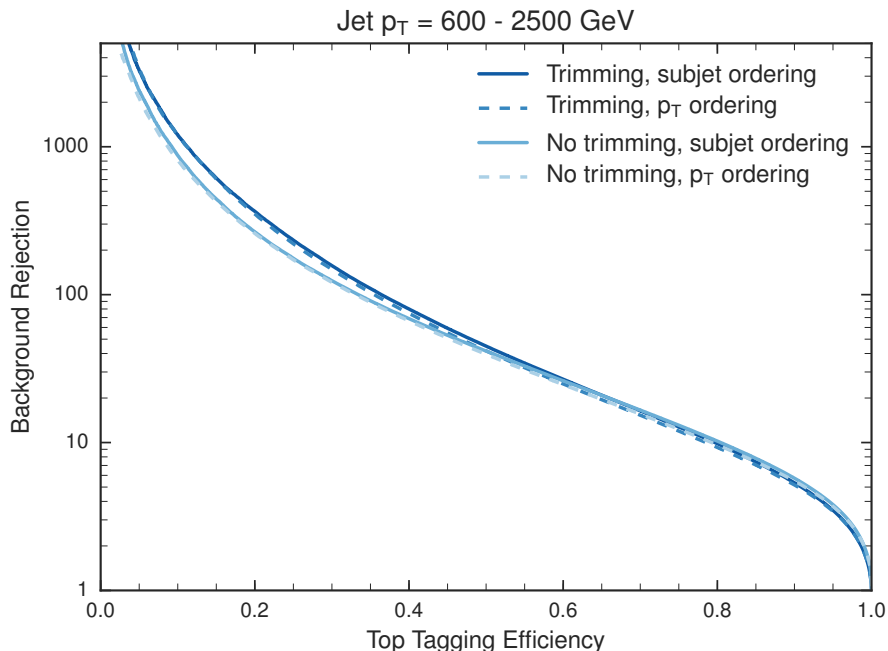


FIG. 8. ROC curve for DNN trained on reconstruction level jets with different trimming and constituent ordering applied. Successive preprocessing stages (scaling, translation, rotation and flipping) are applied for all curves. The LHC 2016 pileup scenario was used.

tested on the data in a given pileup scenario. Testing a network on a pileup level on which it had not been trained is also studied.

Figure 9 shows the performance training and testing on trimmed, reconstructed jets for various levels of pileup. Thanks to the use of inputs from the trimmed jets, the sensitivity to pileup is very small. Figure 10 shows the  $p_T$  dependency on performance under various pileup conditions. The overall trend is that the rejection at low  $p_T$  is best for the high pileup cases, whereas at high  $p_T$  it is approximately 10% better for low pileup scenarios, though again the dependency on pileup is rather small.

Another consideration is whether the DNN would need to be retrained for different pileup scenarios. This does not appear to be the case for the pileup values expected at the LHC Run 2. Figure 11 shows the performance when a network is first trained on one pileup scenario, but then tested on a different scenario. The neural network again appears to be relatively robust against pileup. Indeed the overall performance is almost better for the cases with some pileup. A plausible hypothesis is that pileup essentially adds noise to the data. A common machine learning technique is to augment the data by adding noise, or using dropout [37] to make the DNN more robust to variations, and more able to pick out the salient features required for classification. Thus, deep neural networks maybe be more robust to effects like pileup which essentially mimic more noise, compared to generator or parton showering uncertainties which can greatly affect the jet shapes [17].

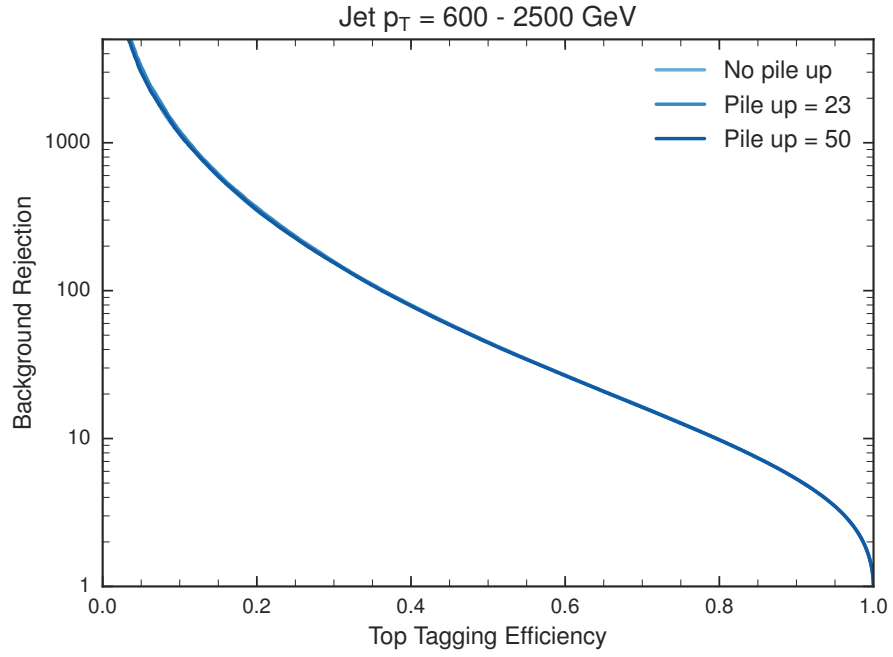


FIG. 9. ROC curve for DNN trained and tested on reconstruction level jet data under different pileup scenarios.

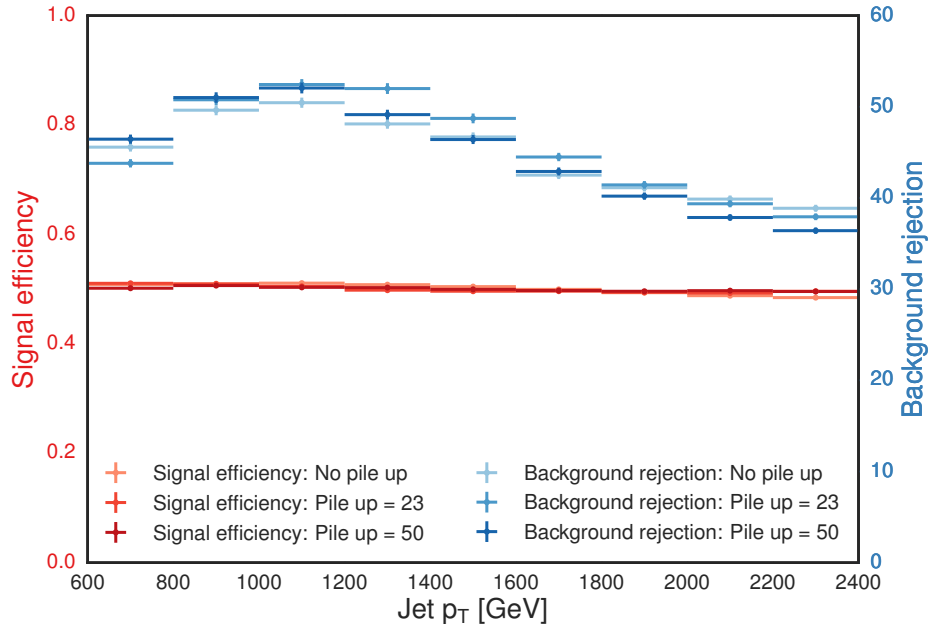


FIG. 10.  $p_T$  dependence of tagger

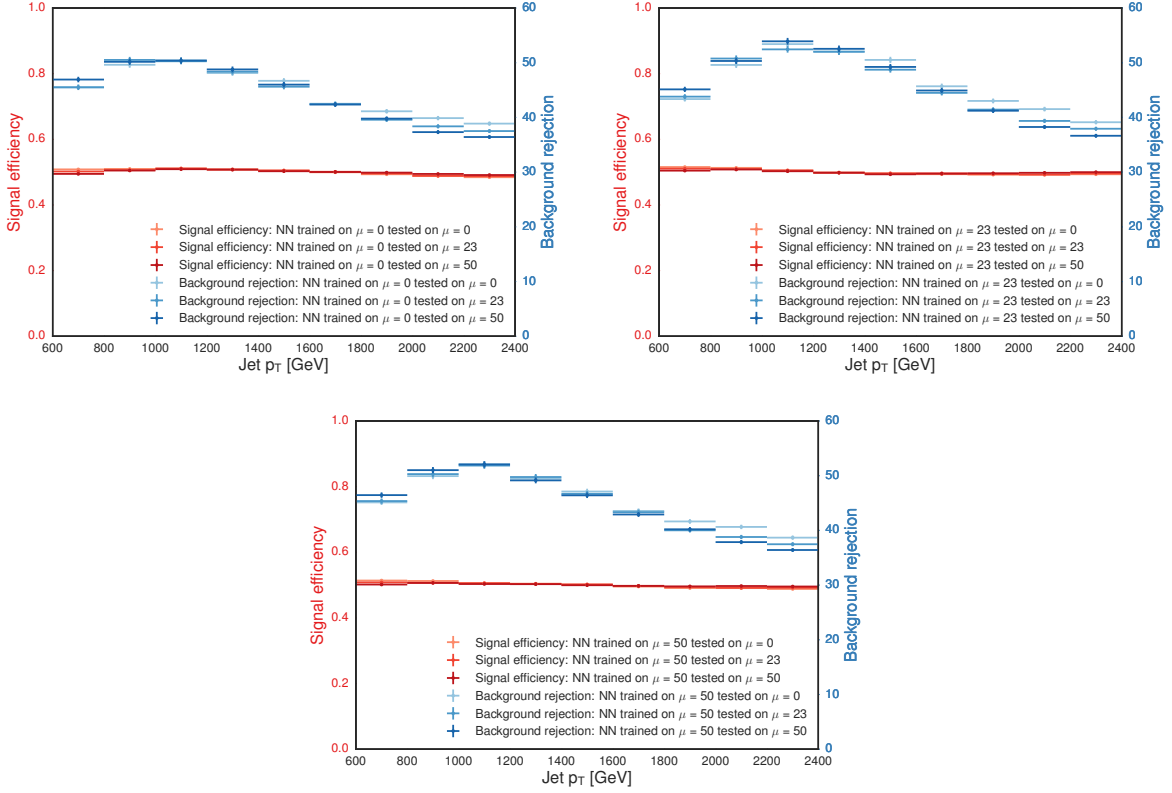


FIG. 11. Effect of training and testing on different pileup levels.

### C. Architecture studies

Network architecture studies were performed within the fully connected network model. Several “rectangular” networks were tried where the number of nodes in a hidden layer was the same for each hidden layer. The depths of such networks varied from 4 to 6 hidden layers with 400 to 1000 nodes in each hidden layer. A larger “tapered” architecture was also tried with one more hidden layer and larger number of nodes per layer (600, 500, 300, 150, 50) with respect to the default network. None of these architectures improved the performance.

Dropout regularization was also attempted on the default network as well as on the larger tapered network. Dropout was applied only on the input layer or only on the hidden layers (with equal dropout probability in each hidden layer) or simultaneously on input and hidden layers with the same dropout probability. Dropout probabilities were varied from 2% to 80% producing no improvement on the performance.

### D. Correlations with high level features

A qualitative evaluation is made if the network has learned to recognize a high level feature known to be important for the classification problem. In Fig. 12 the conditional distribution of jet mass given the network output as well as the conditional distribution of

jet  $p_T$  given the network output are shown. Distributions are presented in a form of two dimensional histograms with the feature of interest on the abscissa and network response on the ordinate. The rows of the histograms are normalized to unity. Both histograms are shown for the background jet sample. The conditional dependence of the jet mass on the network output shows that for the network to classify a background jet as signal-like (output close to 1.0) the jet mass has to be within approximately 30 GeV of the top quark mass. This is the expected behaviour, taking into account the high separation power between signal and background jets that the jet mass (shown in Fig. 13) provides. On the other hand, as desired, there is no similar relationship between the network output and the jet  $p_T$ .

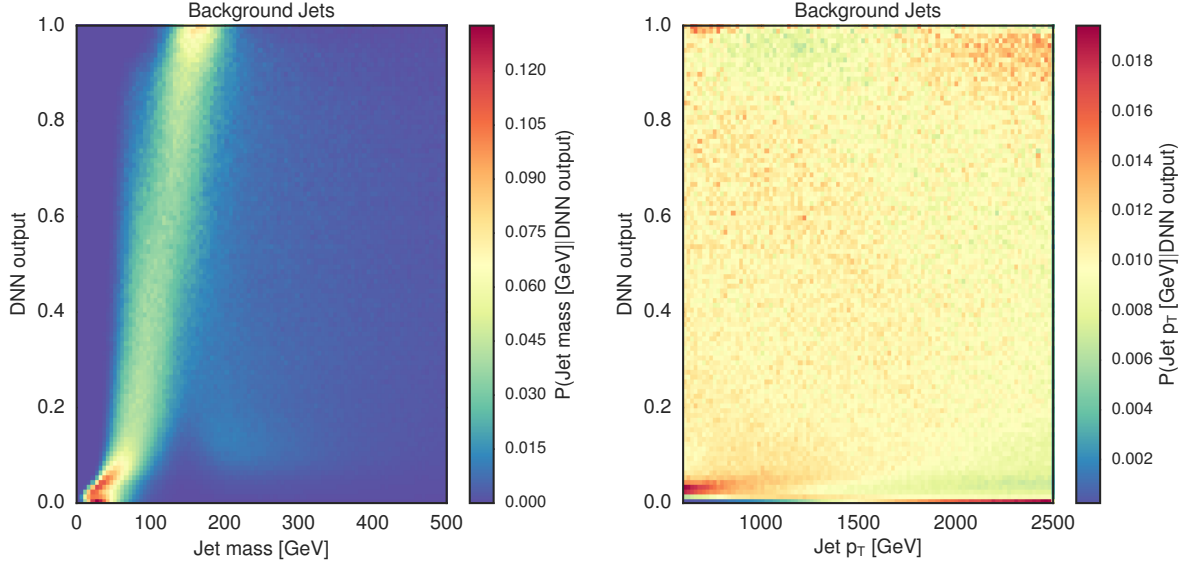


FIG. 12. Conditional distribution of high level jet features on the DNN output. The left plot shows the jet mass, and right plot shows the jet  $p_T$ . Histogram rows have been normalized to unity. The LHC 2016 pileup scenario dataset is used.

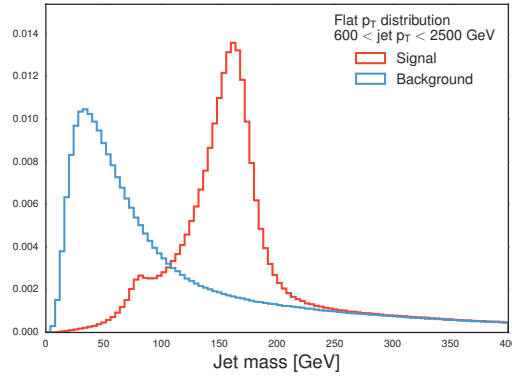


FIG. 13. Distribution of jet mass for the signal and background jet sample. The LHC 2016 pileup scenario dataset is used.



## V. CONCLUSIONS

In this article a method for boosted top quark jet tagging was developed. The method is based on processing a sequence of four vectors of the jet constituents and achieves background rejection of 45 at the 50% efficiency operating point for reconstruction level jets in the  $p_T$  range of 600 to 2500 GeV. The rejection achieved for truth particle jets is 65 at the 50% efficiency operating point. Input ordering and data preprocessing methods preserving jet properties were developed and their importance in achieving high background jet rejection demonstrated. Pileup was found not to substantially influence performance of the classifier. Several methods of jet boosting were found not to further improve DNN's performance. A survey of fully connected network architectures and dropout regularization settings was conducted without resulting performance increase.

The method can be extended in the future to incorporate Recurrent Neural Networks with Long Short-Term Memory [38] that are well-suited for sequence processing. Future directions for this research include the investigation of classifier sensitivity to systematic effects and applying recently developed mitigation methods that incorporate adversarial training [39]. The ultimate goal is the development of a tagger usable in an experimental setting that would have increased performance in comparison with existing top taggers. This would result in higher sensitivity to physics beyond the Standard Model and improved measurements of the Standard Model processes with highly boosted top quarks.

- 
- [1] ATLAS Collaboration, *Search for heavy particles decaying to pairs of highly-boosted top quarks using lepton-plus-jets events in proton-proton collisions at  $\sqrt{s} = 13$  TeV with the ATLAS detector*, ATLAS-CONF-2016-014 (2016), <http://cdsweb.cern.ch/record/2141001>.
  - [2] ATLAS Collaboration, *A search for  $t\bar{t}$  resonances using lepton-plus-jets events in proton-proton collisions at  $\sqrt{s} = 8$  TeV with the ATLAS detector*, JHEP **08** (2015) 148, [arXiv:1505.07018](https://arxiv.org/abs/1505.07018) [hep-ex].
  - [3] C. Collaboration, *Search for resonant  $t\bar{t}$  production in proton-proton collisions at  $\sqrt{s} = 8$  TeV*, Phys. Rev. **D93** (2016) 012001, [arXiv:1506.03062](https://arxiv.org/abs/1506.03062) [hep-ex].
  - [4] CMS Collaboration, *Search for vector-like  $T$  quarks decaying to top quarks and Higgs bosons in the all-hadronic channel using jet substructure*, JHEP **06** (2015) 080, [arXiv:1503.01952](https://arxiv.org/abs/1503.01952) [hep-ex].
  - [5] CMS Collaboration, *Search for single production of vector-like quarks decaying to a  $Z$  boson and a top or a bottom quark in proton-proton collisions at  $\sqrt{s} = 13$  TeV*, [arXiv:1701.07409](https://arxiv.org/abs/1701.07409) [hep-ex].
  - [6] CMS Collaboration, *Search for the production of an excited bottom quark decaying to  $tW$  in proton-proton collisions at  $\sqrt{s} = 8$  TeV*, JHEP **01** (2016) 166, [arXiv:1509.08141](https://arxiv.org/abs/1509.08141) [hep-ex].
  - [7] ATLAS Collaboration, *Measurements of  $t\bar{t}$  differential cross-sections in the all-hadronic channel with the ATLAS detector using highly boosted top quarks in  $pp$  collisions at  $\sqrt{s} = 13$  TeV*, ATLAS-CONF-2016-100 (2016), <http://cdsweb.cern.ch/record/2217231>.
  - [8] ATLAS Collaboration, *Measurement of the differential cross-section of highly boosted top quarks as a function of their transverse momentum in  $\sqrt{s} = 8$  TeV proton-proton collisions using the ATLAS detector*, Phys. Rev. **D93** (2016) 032009, [arXiv:1510.03818](https://arxiv.org/abs/1510.03818) [hep-ex].
  - [9] ATLAS Collaboration, *Search for pair production of heavy vector-like quarks decaying to high- $p_T$   $W$  bosons and  $b$  quarks in the lepton-plus-jets final state in  $pp$  collisions at  $\sqrt{s} = 13$  TeV with the ATLAS detector*, ATLAS-CONF-2016-102 (2016), <http://cdsweb.cern.ch/record/2219436>.
  - [10] ATLAS Collaboration, *Identification of high transverse momentum top quarks in  $pp$  collisions at  $\sqrt{s} = 8$  TeV with the ATLAS detector*, JHEP **06** (2016) 093, [arXiv:1603.03127](https://arxiv.org/abs/1603.03127) [hep-ex].
  - [11] CMS Collaboration, *Boosted Top Jet Tagging at CMS*, CMS-PAS-JME-13-007 (2014), <https://cds.cern.ch/record/1647419>.
  - [12] J. Cogan, M. Kagan, E. Strauss, and A. Schwartzman, *Jet-Images: Computer Vision Inspired Techniques for Jet Tagging*, JHEP **02** (2015) 118, [arXiv:1407.5675](https://arxiv.org/abs/1407.5675) [hep-ph].
  - [13] L. G. Almeida, M. Backovi, M. Cliche, S. J. Lee, and M. Perelstein, *Playing Tag with ANN: Boosted Top Identification with Pattern Recognition*, JHEP **07** (2015) 086, [arXiv:1501.05968](https://arxiv.org/abs/1501.05968) [hep-ph].
  - [14] L. de Oliveira, M. Kagan, L. Mackey, B. Nachman, and A. Schwartzman, *Jet-images – deep learning edition*, JHEP **07** (2016) 069, [arXiv:1511.05190](https://arxiv.org/abs/1511.05190) [hep-ph].

- [15] P. Baldi, K. Bauer, C. Eng, P. Sadowski, and D. Whiteson, *Jet Substructure Classification in High-Energy Physics with Deep Neural Networks*, Phys. Rev. **D93** (2016) 094034, [arXiv:1603.09349 \[hep-ex\]](#).
- [16] D. Guest, J. Collado, P. Baldi, S.-C. Hsu, G. Urban, and D. Whiteson, *Jet Flavor Classification in High-Energy Physics with Deep Neural Networks*, Phys. Rev. **D94** (2016) 112002, [arXiv:1607.08633 \[hep-ex\]](#).
- [17] J. Barnard, E. N. Dawe, M. J. Dolan, and N. Rajcic, *Parton Shower Uncertainties in Jet Substructure Analyses with Deep Neural Networks*, Phys. Rev. **D95** (2017) 014018, [arXiv:1609.00607 \[hep-ph\]](#).
- [18] DELPHES 3 Collaboration, J. de Favereau, C. Delaere, P. Demin, A. Giammanco, V. Lematre, A. Mertens, and M. Selvaggi, *DELPHES 3, A modular framework for fast simulation of a generic collider experiment*, JHEP **02** (2014) 057, [arXiv:1307.6346 \[hep-ex\]](#).
- [19] L. de Oliveira, M. Paganini, and B. Nachman, *Learning Particle Physics by Example: Location-Aware Generative Adversarial Networks for Physics Synthesis*, [arXiv:1701.05927 \[stat.ML\]](#).
- [20] G. Kasieczka, T. Plehn, M. Russell, and T. Schell, *Deep-learning Top Taggers or The End of QCD?*, [arXiv:1701.08784 \[hep-ph\]](#).
- [21] G. Louppe, K. Cho, C. Becot, and K. Cranmer, *QCD-Aware Recursive Neural Networks for Jet Physics*, [arXiv:1702.00748 \[hep-ph\]](#).
- [22] J. S. Conway, R. Bhaskar, R. D. Erbacher, and J. Pilot, *Identification of High-Momentum Top Quarks, Higgs Bosons, and W and Z Bosons Using Boosted Event Shapes*, Phys. Rev. **D94** (2016) 094027, [arXiv:1606.06859 \[hep-ex\]](#).
- [23] F. Chollet, *Keras*, <https://github.com/fchollet/keras>.
- [24] Theano Development Team, *Theano: A Python framework for fast computation of mathematical expressions*, [arXiv:1501.05968 \[cs.SC\]](#).
- [25] ATLAS Collaboration, *ATLAS Pythia 8 tunes to 7 TeV data*, ATL-PHYS-PUB-2014-021, 2014, <http://cds.cern.ch/record/1966419>.
- [26] T. Sjstrand, S. Ask, J. R. Christiansen, R. Corke, N. Desai, P. Ilten, S. Mrenna, S. Prestel, C. O. Rasmussen, and P. Z. Skands, *An introduction to PYTHIA 8.2*, Computer Physics Communications **191** (2015) 159 – 177, [arXiv:1510.03818 \[hep-ph\]](#).
- [27] A. Buckley, J. Ferrando, S. Lloyd, K. Nordström, B. Page, M. Rüfenacht, M. Schönherr, and G. Watt, *LHAPDF6: parton density access in the LHC precision era*, The European Physical Journal C **75** (2015) 132, [arXiv:1412.7420 \[hep-ph\]](#).
- [28] P. Langacker, *The Physics of Heavy  $Z'$  Gauge Bosons*, Rev. Mod. Phys. **81** (2009) 1199–1228, [arXiv:0801.1345 \[hep-ph\]](#).
- [29] CMS Collaboration, *Particle-Flow Event Reconstruction in CMS and Performance for Jets, Taus, and Emiss*, CMS-PAS-PFT-09-001, 2009, <https://cds.cern.ch/record/1194487>.
- [30] CMS Collaboration, *Commissioning of the particle-flow event reconstruction with the first LHC collisions recorded in the CMS detector*, CMS-PAS-PFT-10-001, 2010, <https://cds.cern.ch/record/1247373>.
- [31] M. Cacciari, G. P. Salam, and G. Soyez, *The anti- $k_t$  jet clustering algorithm*, Journal of High

- Energy Physics **2008** (2008) 063, [arXiv:0802.1189](#) [hep-ph].
- [32] M. Cacciari, G. P. Salam, and G. Soyez, *FastJet User Manual*, Eur. Phys. J. **C72** (2012) 1896, [arXiv:1111.6097](#) [hep-ph].
  - [33] D. Krohn, J. Thaler, and L.-T. Wang, *Jet Trimming*, JHEP **02** (2010) 084, [arXiv:0912.1342](#) [hep-ph].
  - [34] S. Catani, Y. L. Dokshitzer, M. H. Seymour, and B. R. Webber, *Longitudinally invariant  $K_t$  clustering algorithms for hadron hadron collisions*, Nucl. Phys. **B406** (1993) 187–224.
  - [35] V. Nair and G. E. Hinton, *Rectified Linear Units Improve Restricted Boltzmann Machines*, Proceedings of the 27th International Conference on Machine Learning (ICML-10) (2010) 807–814, <http://www.icml2010.org/papers/432.pdf>.
  - [36] D. P. Kingma and J. Ba, *Adam: A Method for Stochastic Optimization*, [arXiv:1412.6980](#) [cs.LG].
  - [37] G. E. Hinton, N. Srivastava, A. Krizhevsky, I. Sutskever, and R. Salakhutdinov, *Improving neural networks by preventing co-adaptation of feature detectors*, [arXiv:1207.0580](#) [cs.NE].
  - [38] S. Hochreiter and J. Schmidhuber, *Long Short-Term Memory*, Neural Computation **9** (1997) 1735–1780.
  - [39] G. Louppe, M. Kagan, and K. Cranmer, *Learning to Pivot with Adversarial Networks*, [arXiv:1611.01046](#) [stat.ME].